ELSEVIER

Journal of Alloys and Compounds 234 (1996) 130–136

Journal of ALLOYS AND COMPOUNDS

Regularities of melting behavior of some binary alloy phases. Part 2. Computerized prediction of melting points of alloy phases

Chen Nianyi, Li Chonghe, Yao Shuwen, Wang Xueye

Shanghai Institute of Metallurgy, Academia Sinica, 200050 Shanghai, People®s Republic of China

Received 10 November 1994; in final form 2 May 1995

Abstract

Melting point regularities of Laves phases, CsCl-type and $AuCu_3$-type alloy phases have been investigated by use of an artificial neural network using atomic parameters and known data for the melting points of these alloy phases as inputs. The adjusted artificial neural network can be used for quantitative prediction of the melting points of these alloy phases, with an average error of about 6%.

Keywords: Melting point; Computerized prediction; Artificial neural network

1. Introduction

One of the most difficult problems in the computerized prediction of the phase diagrams of alloy systems is that of the melting points (or the decomposition temperature in incongruent melting) of intermediate phases. Some work has been done in this field. For example, Hulliger and Villars [1] have studied the regularities of the melting points of AB-type alloy phases. Walzer [2] has proposed a diagrammatic method to investigate the regularities of the melting points of intermetallic compounds. Although some rules have been found, a generally applicable, quantitative method for melting point prediction has not yet been obtained. Since it is well known that the melting process is influenced by many factors described by atomic parameters, and that the artificial neural network (ANN) is an effective tool for the investigation and prediction of complicated phenomena affected by many factors [3], it would seem reasonable to use ANN and atomic parameters for the investigation and prediction of the melting points of alloy phases.

2. Model and method of computation

2.1. Model for the influence of atomic parameters on melting points of alloy phases

The melting point of a substance is determined by the free-energy change of the phase transformation from the crystalline to the liquid state, hence any atomic parameter affecting the energy or entropy difference between each state will influence the melting point of the substance. For a binary alloy phase A_mB_n ($n \geq m$) whose atom A is predominantly surrounded by atom B (Laves phases, CsCl-type and $AuCu_3$-type alloy phases all belong to this category), larger electronegativity differences ΔX between A and B should make A and B bear electric charges of opposite sign. This should favor the stability of the crystal lattice. The randomization induced by the melting process will lead to the breakdown (at least to some degree) of the chemical order between A and B and thus increase the contact between atoms bearing the same sign of electric charge, so it is reasonable to imagine that a larger ΔX will make the melting point higher. Another atomic parameter Δn_{ws} proposed by Miedema [4], representing the valence electron density difference between the Wagner–Seitz cells of A and B atoms in alloy phases, should also influence the stability of the crystal lattice of alloy phases. Larger Δn_{ws} values destabilize the crystal lattice and should make the melting point lower. Yet another atomic parameter that should affect the lattice stability is the geometric factor, represented by R_A, R_B, or R_A/R_B. The optimal effective radius ratio of the A and B (which is dependent on ΔX or the charge transfer between A and B, as indicated in Part 1 of this series [5]) for every crystal-type should give the closest packing with

SSDI 0925-8388(95)01963-4

highest lattice stability and the highest melting point of alloy phases. Besides, the valence electron numbers Z_A and Z_B, or the valency electron / atom ratio e/a (both of which are related to the energy band of the alloy phases) should also be factors affecting the lattice stability and hence the melting point of alloy phases. All of the above-mentioned parameters or their functions may be useful for the investigation of the melting point regularities of alloy phases.

2.2. Selection of the optimal group of atomic parameters as the inputs of ANN

A series of atomic parameters have been tested as the best set of inputs for ANN. Three-hundred-and-ninety-eight known alloy phases were used as test samples for the investigation of the regularities of melting point of alloy phases, in order to find the set of atomic parameters most capable of correlation and prediction. The best parameter set found was the following: ΔX, R_A/R_B, $\Delta(Z/R^3)$ (an approximate expression for Δn_{ws}), e/a (the valence electron / atom ratio) and the melting points of the constituent elements.

2.3. Structure and function of ANN used in this work

An ANN is a directed graph with nodes for the simulation of the structure and function of human neural networks [3]. The ANN composed of three types of units is shown in Fig. 1 (input units a_i $(1 \leqslant i \leqslant n)$, hidden units h_j $(1 \leqslant j \leqslant s)$ and output units d_k $(1 \leqslant k \leqslant m)$) is a back-propagation (B-P) network. In the B-P network both hidden units and output units are non-linear; only the input node is linear. The non-linear activation function in B-P model is generally a sigmoid function:

$$f(X) = 1/(1 + e^{-X})$$

The numbers of nodes and layers are dependent on the domain concerned. The neuron in each layer is connected to every neuron in the upper and lower layers, and the strength of connection is determined by the weight W on the connecting line. W_{ji} represents the connecting weight of neuron U_i to U_j. Each adjustment period of the B-P algorithm given by Rumelhart consists two phases:

(1) The input parameter is transmited to the hidden node and is activated by the sigmoid function; its output signal is subsequently transmitted to the output layer. Let $\text{net}k_i^p$ represent the pth sample in the input of the ith node, then:

$$\text{net}k_i^{kij} = \Sigma W_{kij} \times O_{k-1,j} + \theta_{ki}$$

in which θ_{ki} is the threshold of ith node of the kth layer, $O_{k-1,j}$ is the output of the jth node of the $(k-1)$th layer, and W_{kij} is the connecting weight between the ith node of the kth layer and the jth node of the $(k-1)$th layer.

$$O_{ki}^p = f(\text{net}k_j^p)$$

(2) Errors back-propagated: errors function $E_p^p = 1/2\Sigma(T_j - O_{lj})^2$ (assume l is output layer), where T_j^p represents the pth model in the target output of the jth node. Let ΔE represent the error function related to the gradient of weight W, then the error-correction formula is:

$$W^{(k+1)} = W^{(k)} - \eta_k \Delta E(W^{(k)})$$

η_k is an adjustable constant, its selected value related directly to the speed of convergence. The error minimizing process of the B-P network is based on the gradient descent method. η_k is generally selected to be a random small value. Based on the above principle a typical ANN used in this work is illustrated in Fig. 2. The atomic parameters together with the melting point data for the constituent elements are used as inputs, and the melting point or melting point deviation from the linear average, ΔT, is used as the output. By some typical transfer functions such as $\tan hx$ or a sigmoid function, the weights w_{ji} are adjusted to fit the test sets consisting of the data for known alloy phases. If a set

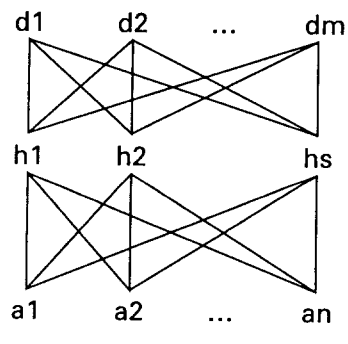

Fig. 1. The ANN composed of three types of units.

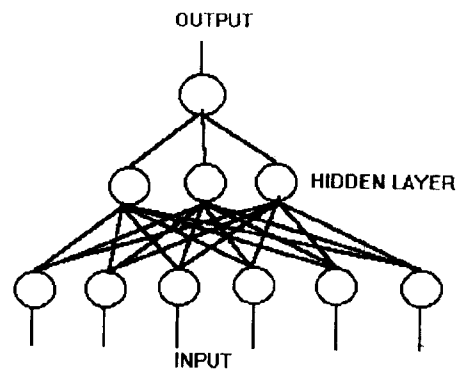

Fig. 2. A typical ANN.

of suitable w_{ji} values have been selected to fit a large number of known data very well, i.e. if the correlated values agree closely with the experimental values, it may be concluded that some regularities have definitely been found. The ANN program of NeuralWare Inc. (USA) is used in our computation. The adjusted ANN can be used for the estimation or rough prediction of the unknown melting points of alloy phases.

3. Results of computations

3.1. Melting point regularities and melting point predictions for Laves phases

The melting points of C14- and C15-types of Laves phase measured before 1986 (data published in Ref. [6]) were used as the test set. They are listed in Table

Table 1
The Laves phase samples studied[a]

No.	Compd.	C.T.[b]	M.T.[c]	T_{exp}(k)	$T_p(T_c)$(k)[d]	No.	Compd.	C.T.[b]	M.T.[c]	T_{exp}(k)	$T_p(T_c)$(k)[d]	No.	Compd.	C.T.[b]	M.T.[c]	T_{exp}(k)	$T_p(T_c)$(k)[d]
1	$CaLi_2$	C14	C	508	603	52	$CaAl_2$	C15	C	1352	1411	103	$CeNi_2$	C15	I	1103	1174
2	$MgZn_2$	C14	C	863	866	53	UMn_2	C15	C	1393	1364	104	$SmFe_2$	C15	I	1173	1256
3	$CaAg_2$	C14	C	868	900	54	UCo_2	C15	C	1443	1562	105	$PrNi_2$	C15	I	1183	1225
4	$BaMg_2$	C14	C	880	941	55	$ZrZn_2$	C15	C	1453	1517	106	$DyMn_2$	C15	I	1203	1296
5	$SrMg_2$	C14	C	953	906	56	$ScAl_2$	C15	C	1468	1673	107	$PrCo_2$	C15	I	1204	1231
6	$YbCd_2$	C14	C	976	983	57	UCo_2	C15	C	1473	1562	108	$CeFe_2$	C15	I	1205	1152
7	$CaMg_2$	C14	C	988	958	58	$CuBe_2$	C15	C	1492	1467	109	$NdNi_2$	C15	I	1213	1256
8	$YbMg_2$	C14	C	991	943	59	$PuFe_2$	C15	C	1513	1491	110	$GdMn_2$	C15	I	1223	1275
9	$EuMg_2$	C14	C	992	919	60	$TmFe_2$	C15	C	1573	1617	111	$HoMn_2$	C15	I	1238	1263
10	$TiMn_2$	C14	C	1598	1605	61	$CaPd_2$	C15	C	1573	1444	112	$NdCo_2$	C15	I	1238	1322
11	$ZrMn_2$	C14	C	1613	1564	62	$PuCo_2$	C15	C	1573	1569	113	UNi_2	C15	I	1258	1389
12	$TiFe_2$	C14	C	1700	1734	63	$ScNi_2$	C15	C	1583	1532	114	$AgBe_2$	C15	I	1283	1364
13	$NbCo_2$	C14	C	1753	1762	64	$LuFe_2$	C15	C	1618	1572	115	$PrFe_2$	C15	I	1303	1191
14	$NbMn_2$	C14	C	1793	1839	65	$YbAl_2$	C15	C	1633	1697	116	$SmNi_2$	C15	I	1307	1279
15	$NbFe_2$	C14	C	1900	1889	66	$ErFe_2$	C15	C	1633	1597	117	$CeCo_2$	C15	I	1308	1179
16	$HfAl_2$	C14	C	1923	1939	67	$LaAl_2$	C15	C	1678	1679	118	$CaNi_2$	C15	I	1308	1310
17	$TaFe_2$	C14	C	2048	2041	68	$NdRh_2$	C15	C	1688	1957	119	$GdNi_2$	C15	I	1343	1392
18	$DyRu_2$	C14	C	2073	2103	69	$PrAl_2$	C15	C	1691	1702	120	$SmCo_2$	C15	I	1347	1286
19	VBe_2	C14	C	2073	2086	70	$ErAl_2$	C15	C	1728	1737	121	$GdFe_2$	C15	I	1353	1367
20	$CrBe_2$	C14	C	2077	2006	71	$NdAl_2$	C15	C	1733	1717	122	$GdCo_2$	C15	I	1373	1394
21	YRu_2	C14	C	2223	2143	72	$CeAl_2$	C15	C	1753	1674	123	$CdCo_2$	C15	I	1373	1241
22	$MoBe_2$	C14	C	2300	2346	73	$FeBe_2$	C15	C	1753	1650	124	YNi_2	C15	I	1388	1484
23	URe_2	C14	C	2473	2504	74	YAl_2	C15	C	1758	1788	125	YFe_2	C15	I	1398	1462
24	WBe_2	C14	C	2523	2497	75	$SmAl_2$	C15	C	1773	1977	126	$NdFe_2$	C15	I	1403	1233
25	$ThRe_2$	C14	C	2773	2896	76	$PuOs_2$	C15	C	1773	1775	127	$TbFe_2$	C15	I	1460	1385
26	$ZrOs_2$	C14	C	2933	2956	77	$DyAl_2$	C15	C	1773	1724	128	$TiCo_2$	C15	I	1508	1520
27	$HfOs_2$	C14	C	3023	3149	78	$ScCo_2$	C15	C	1793	1556	129	$YbNi_2$	C15	I	1528	1245
28	$HfRe_2$	C14	C	3433	3230	79	$GdAl_2$	C15	C	1798	1805	130	$ErNI_2$	C15	I	1528	1487
29	KNa_2	C14	I	280	285	80	$HoAl_2$	C15	C	1803	1759	131	$DyNi_2$	C15	I	1531	1430
30	KPb_2	C14	I	611	608	81	$PuAl_2$	C15	C	1813	1742	132	$HoFe_2$	C15	I	1561	1438
31	$HoMg_2$	C14	I	923	930	82	HfV_2	C15	C	1823	1868	133	$HoCo_2$	C15	I	1573	1467
32	$LuMg_2$	C14	I	923	976	83	$PuRu_2$	C15	C	1833	1757	134	$TiBe_2$	C15	I	1623	1576
33	$ErMg_2$	C14	I	983	939	84	UAl_2	C15	C	1863	1662	135	$LaRu_2$	C15	I	1704	1787
34	$TmMg_2$	C14	I	993	947	85	$ZrCo_2$	C15	C	1873	1914	136	$PuPt_2$	C15	I	1853	1823
35	$TbMn_2$	C14	I	1185	1211	86	$TmAl_2$	C15	C	1895	1721	137	$TaCo_2$	C15	I	1866	1878
36	$NdMn_2$	C14	I	1193	1197	87	$HfCo_2$	C15	C	1943	2024	138	$NbBe_2$	C15	I	1903	1878
37	$SmMn_2$	C14	I	1203	1204	88	$ZrCr_2$	C15	C	1946	2047	139	UIr_2	C15	I	2133	2127
38	$MgCo_2$	C14	I	1243	1233	89	$ZrFe_2$	C15	C	1948	1892	140	$ZrMo_2$	C15	I	2153	2130
39	$ErMn_2$	C14	I	1263	1233	90	YOs_2	C15	C	2423	2380	141	$ZrIr_2$	C15	I	21358	2272
40	$ScRu_2$	C14	I	2113	2139	91	$CeIr_2$	C15	C	2523	2501	142	ZrW_2	C15	I	2483	2619
41	$ZrRu_2$	C14	I	2233	2211	92	UOs_2	C15	C	2553	2324	143	HfW_2	C15	I	2785	2693
42	$TbRe_2$	C14	I	2723	2748	93	$LaIr_2$	C15	C	2793	2569	114	$DyMg_2$*	C14	I	983	920
43	$ZrRe_2$	C14	I	2723	2738	94	$BiAu_2$	C15	I	644	664	145	YMg_2*	C14	I	1055	938
44	YRe_2	C14	I	2793	2747	95	$PbAu_2$	C15	I	707	739	146	$NdMg_2$*	C15	I	1043	1029
45	KBi_2	C15	C	838	844	96	$CeMg_2$	C15	I	1023	1000	147	$HoNi_2$*	C15	I	1468	1475
46	$CsBi_2$	C15	C	868	842	97	$EuPt_2$	C15	I	1043	1087	148	$LaRh_2$*	C15	I	1668	1482
47	$RbBi_2$	C15	C	878	848	98	$CeFe_2$	C15	I	1046	1152	149	YCo_2*	C15	I	1427	1482
48	$MgCu_2$	C15	C	1070	1054	99	$LaMg_2$	C15	I	1048	1017	150	$LuAl_2$*	C15	C	1773	1673
49	$PuZn_2$	C15	C	1208	1416	100	$PrMg_2$	C15	I	1053	1019	151	$NdRu_2$*	C15	I	1923	1900
50	$NaAu_2$	C15	C	1275	1138	101	$GdMg_2$	C15	I	1083	1111	152	$SmRu_2$*	C15	C	2193	2260
51	$PuMn_2$	C15	C	1323	1340	102	$LeNi_2$	C15	I	1100	1229						

[a] Alloy phases whose melting points were measured after 1987 are not included in our test set. They are used as the subjects of melting point predictions.
[b] C.T. crystal type: C14, $MgZn_2$; C15 $MgCu_2$.
[c] M.T. melting type: c, congruent; I, incongruent.
[d] T_p predicted m.p.; T_c correlated m.p.

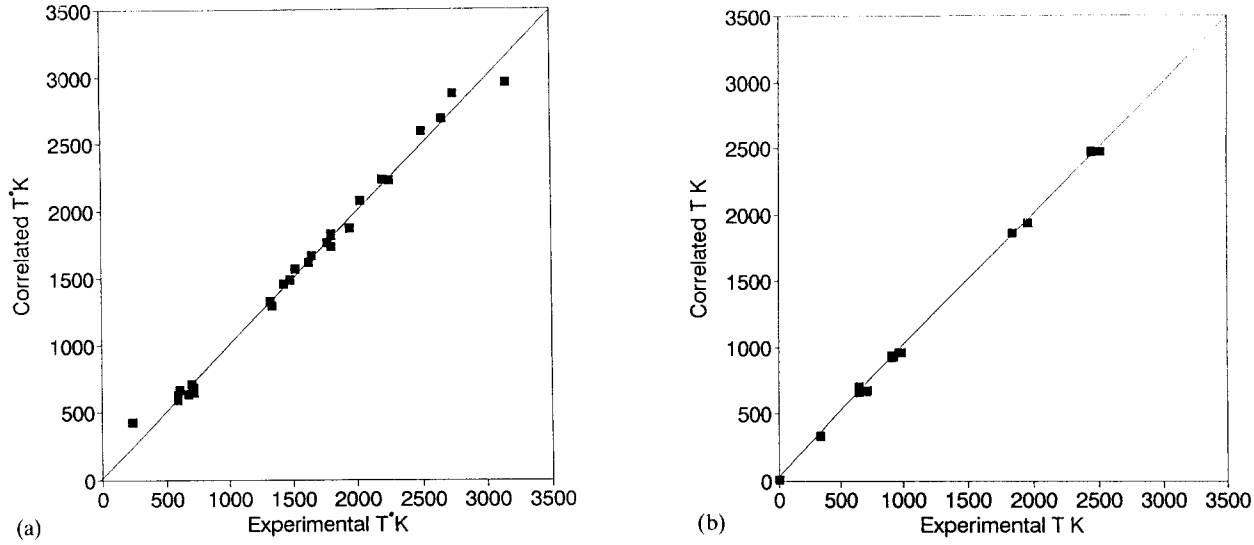

Fig. 3. Correlation the between melting point data of C14 phases: (a) congruently melting phases; (b) incongruently melting phases.

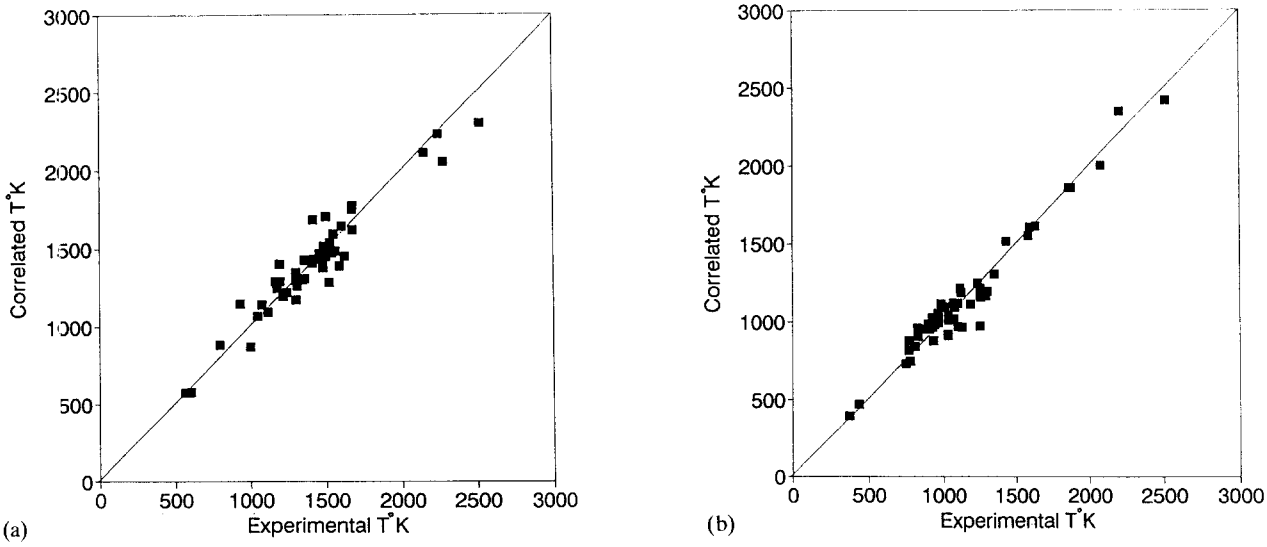

Fig. 4. Correlation between the melting point data of C15 phases: (a) congruently melting phases; (b) incongruently melting phases.

1 (samples without *). Figs. 3(a) and 3(b) illustrate the comparison of the experimental melting point data and the correlated values of the congruently and incongruently melting C14-type Laves phases, respectively. Figs. 4(a) and 4(b) compare the experimental melting point data and the correlated values for the congruently and incongruently melting C15-type Laves phases, respectively. It can be seen that the correlated and experimental data are rather close to each other, implying that some regularity exists. Some melting point data for newly discovered Laves phases published after 1987 were used to test the ability of prediction of the adjusted ANN. The melting points of the newly discovered $DyMg_2$, YMg_2, $NdMg_2$, $HoNi_2$, $LaRh_2$, YCo_2, $LuAl_2$, $NdRu_2$ and $SmRu_2$ were the subjects of computerized prediction.

Fig. 5. compares the experimental data and the predicted values. The agreement is rather good., with an average error of only 5.7% of the average melting point data.

3.2. Melting point regularity and melting point prediction for CsCl-type alloy phases

Since most CsCl-type alloy phases exhibit congruent melting, only the congruent melting point data have been investigated here. The data for CsCl-type alloy phases known before 1986 listed in Table 2are used as training set. Fig. 6 compares the experimental data and the correlated values for these alloy phases, while Fig. 7 illustrates the results of computerized prediction of the melting points of 36 newly discovered CsCl-type

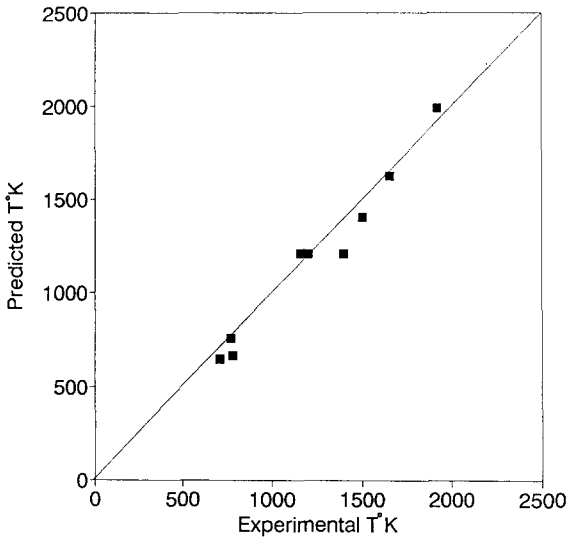

Fig. 5. Comparison between the experimental melting point data and the computerized predictions for nine newly discovered Laves phases.

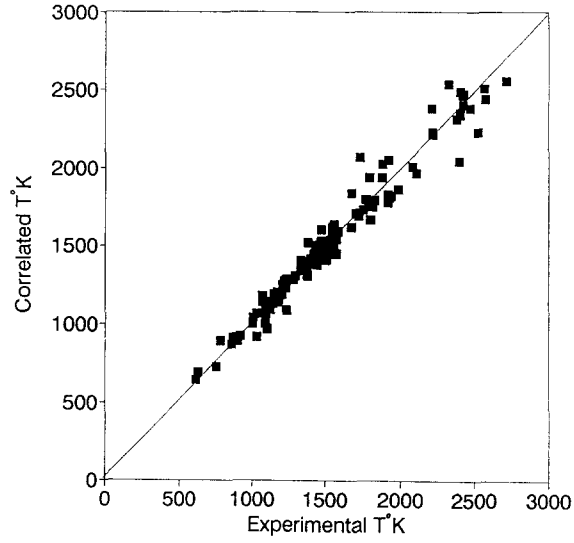

Fig. 6. Correlation between the melting point data of CsCl-type alloy phases.

Table 2
CsCl-type phase used[a]

No.	Compd.	T_{exp}(K)	$T_p(T_c)$	No.	Compd.	T_{exp}(K)	$T_p(T_c)$	No.	Compd.	T_{exp}(K)	$T_p(T_c)$	No.	Compd.	T_{exp}(K)	$T_p(T_c)$
1	BaZn	613	646	39	GdIn	1523	1520	77	YHg	1473	1602	115	HfIr	2713	2557
2	MgTl	631	694	40	BeCo	1703	1708	78	NdAg	1225	1231	116	HoIr	2573	2442
3	LiPb	755	724	41	TmCu	1373	1369	79	YCd	1473	1483	117	ScNi	1543	1618
4	BaCd	861	869	42	LaAg	1153	1188	80	YbCd	1069	1176	118	TiNi	1583	1590
5	LiHg	868	911	43	YbHg	1373	1313	81	TbHg	1473	1528	119	TiPd	1673	1837
6	MgHg	900	894	44	CaPd	1183	1161	82	NdTl	1553	1483	120	Zrco	1673	1616
7	LiAu	918	922	45	GdAg	1373	1391	83	BePd	1728	2068	121	YPd	1723	1692
8	BeAu	1003	1004	46	PrAg	1205	1189	84	CeTl	1483	1480	122	DyPd	1723	1695
9	ZnAu	1031	916	47	GaCo	1377	1519	85	SmIn	1483	1428	123	HoPd	1753	1731
10	MgAg	1093	1065	48	HoIn	1543	1571	86	NdHg*	1423	1390	124	MnPd	1788	1761
11	BaHg	1095	1118	49	YZn	1378	1301	87	PrAu*	1688	1560	125	ErRh	1793	1937
12	SrHg	1123	1094	50	LaCd	1219	1271	88	NdAu*	1723	1624	126	ErPd	1813	1748
13	CaIn	1168	1175	51	ScAg	1503	1442	89	TmZn*	1403	1385	127	TbRh	1823	1792
14	SrTl	1179	1138	52	DyCu	1228	1270	90	GdAu*	1858	1768	128	ScPd	1873	1940
15	CaHg	1234	1284	53	NdIn	1503	1410	91	DyHg*	1443	1551	129	HfCo	1913	1830
16	MgAu	1423	1445	54	SmAg	1232	1269	92	TbAu*	1896	1793	130	YRh	1923	1808
17	LiTl	783	894	55	ScCu	1398	1414	93	YbTl*	1400	1490	131	TiPt	2103	1968
18	AlIr	2393	2047	56	DyAu	1933	1820	94	HoAu*	1971	1845	132	ZrRh	2208	2379
19	ThBi	2073	2006	57	CeIn	1413	1389	95	SmHg*	1473	1413	133	TiRh	2213	2231
20	ScAl	1573	1443	58	AlCo	1913	1776	96	TmAu*	1993	1870	134	NbRu	2215	2215
21	DyIn	1573	1547	59	TbAg	1418	1429	97	HoTl*	1503	1636	135	ZrIr	2323	2535
22	SmZn	1233	1085	60	LaZn	1088	1001	98	SiRu*	2023	2054	136	ZrPt	2377	2315
23	GdTl	1543	1590	61	YAg	1433	1501	99	DyTl*	1573	1613	137	TiRu	2403	2342
24	ErAu	1983	1861	62	GdCu	1103	1138	100	LaAu*	2053	1903	138	TiIr	2403	2349
25	HoCu	1283	1284	63	HoAg	1438	1493	101	TbZn*	1373	1246	139	ZrRu	2403	2487
26	SmCu	1008	1041	64	CeAg	1143	1131	102	CaCd*	958	1100	140	TiOs	240	2467
27	SmCd	1296	1305	65	GdCd	1443	1397	103	ErZn*	1423	1365	141	YIr	2423	2404
28	EuCd	1033	1065	66	InPd	1558	1632	104	CaTl*	1253	1293	142	ErIr	2423	2469
29	TbIn	1533	1532	67	PrIn	1443	1377	105	HoHg*	1443	1572	142	ScRu	2473	2384
30	AlNi	1911	1795	68	YCu	1208	1243	106	LuZn*	1373	1447	144	ScPt	2523	2228
31	ErCu	1328	1338	69	DyAg	1455	1457	107	SmTl*	1493	1497	145	HfRh	2563	2506
32	SmMg	1073	1137	70	DyCu	1228	1227	108	DyZn*	1338	1276	146	HoZn*	1373	1323
33	LaHg	1333	1405	71	ErAg	1468	1519	109	TbTl*	1573	1599	147	PrZn*	1155	1019
34	BeNi	1878	2026	72	AlPd	1918	2051	110	GdZn*	1323	1191	148	TiCo*	1598	1511
35	YbIn	1340	1384	73	GdHg	1473	1513	111	YbAg*	997	1079	149	GdRh*	1743	1730
36	CeZn	1098	968	74	SmAu	1798	1664	112	NdZn*	1196	1049	150	TmPd*	1843	1777
37	PrTl	1533	1448	75	LuCu	1473	1437	113	YbAu*	1565	1403	151	TmIr*	2473	2471
38	TiAu	1768	1795	76	TbCu	1173	1198	114	PrHg*	1373	1352	152	HfRu*	2673	2544

[a] See footnotes [a] and [d], Table 1.

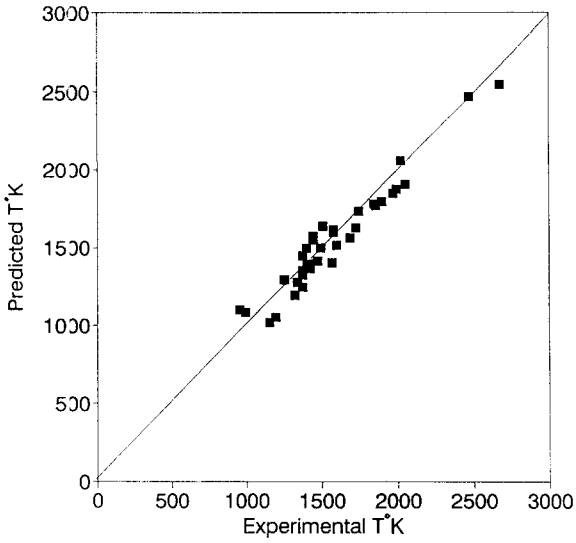

Fig. 7. Computerized predictions of the melting points of 36 newly discovered CsCl-type alloy phases.

alloy phases. These newly discovered phases include CaTl, NdHg, TiCo, etc., as indicated in Table 2 by the * sign. (These newly discovered phases are not included in the test set.) The results of the prediction are rather good, with an average error of 5.3% of the average melting point.

3.3. Melting point regularity and melting point prediction of $AuCu_3$-type alloy phases

Table 3 lists the melting point data of $AuCu_3$-type alloy phases measured before 1986 (used as a test set), and that of the newly discovered $AuCu_3$-type alloy phases (used as the subject of computerized prediction). Figs. 8(a) and 8(b) compare the experimental data and the correlated values for congruently and incongruently melted $AuCuR_3$-type alloy phases, respectively. The melting points of nine newly discovered $AuCu_3$-type alloy phases, including $NdTl_3$,

Table 3
$AuCu_3$-type phases used[a]

No.	Compd.	M.T.	T_{exp} (K)	$T_p(T_c)$	No.	Compd.	M.T.	T_{exp} (K)	$T_p(T_c)$	No.	Compd.	M.T.	T_{exp} (K)	$T_p(T_c)$
1	$SrBi_3$	C	903	1059	33	$NdIn_3$	C	1493	1391	65	$GaLa_3$	I	873	993
2	$BiCs_3$	C	908	995	34	UPb_3	C	1493	1612	66	$GaNd_3$	I	1059	1028
3	$CaPb_3$	C	939	1143	35	$PbPd_3$	C	1493	1541	67	$GaPr_3$	I	959	939
4	$YbPb_3$	C	1013	1249	36	$EuPd_3$	C	1688	1702	68	$GaSm_3$	I	1148	1035
5	$EuPb_3$	C	1061	1224	37	$SnPt_3$	C	1693	1553	69	$GdPb_3$	I	1242	1110
6	$YbSn_3$	C	1078	1203	38	$CePd_3$	C	1710	1722	70	$InCe_3$	I	1193	1096
7	$GdTl_3$	C	1263	1357	39	UGe_3	C	1748	1674	71	$InLa_3$	I	1089	1092
8	$PrTl_3$	C	1323	1363	40	$PuPd_3$	C	1773	1733	72	$InNd_3$	I	1203	1096
9	$TmIn_3$	C	1333	1395	41	$GdPd_3$	C	1903	1866	73	$InPr_3$	I	1040	1087
10	$SmPb_3$	C	1333	1357	42	$TbPd_3$	C	1943	1887	74	$LuGa_3$	I	1203	1204
11	$SmSn_3$	C	1363	1309	43	YPd_3	C	1973	1944	75	$PbPu_3$	I	1169	1179
12	$ErIn_3$	C	1363	1390	44	$YbPd_3$	C	1973	1714	76	$ScGa_3$	I	1303	1313
13	$LaTl_3$	C	1369	1270	45	$DyPd_3$	C	1983	1910	77	$ScIn_3$	I	1183	1119
14	YIn_3	C	1383	1376	46	$ErPd_3$	C	1983	1955	78	$SnPu_3$	I	1143	1164
15	$HoIn_3$	C	1383	1389	47	$HoPd_3$	C	2003	1934	79	$ThPb_3$	I	1138	1190
16	$PrPb_3$	C	1388	1355	48	URh_3	C	2123	2070	80	$ThSn_3$	I	1228	1197
17	$GeNi_3$	C	1403	1465	49	$TiPt_3$	C	2233	2241	81	$TiZn_3$	I	923	938
18	$SmIn_3$	C	1403	1394	50	$HfRh_3$	C	2278	2488	82	$TlNd_3$	I	1068	1100
19	$PuPb_3$	C	1411	1395	51	UIr_3	C	2278	2420	83	$TmGa_3$	I	1233	1195
20	$TbIn_3$	C	1413	1388	52	$TaRh_3$	C	2398	2566	84	UAl_3	I	1625	1626
21	$LaIn_3$	C	1413	1302	53	$ZrIr_3$	C	2553	2494	85	UGa_3	I	1523	1534
22	$PrSn_3$	C	1418	1307	54	$HfIr_3$	C	2733	2488	86	$NdTl_3$*	C	1388	1361
23	$LaSn_3$	C	1420	1215	55	$NbIr_3$	C	2773	2700	87	$MdSn_3$*	C	1411	1306
24	$DyIn_3$	C	1423	1389	56	YPb_3	I	1013	1113	88	$ZrRh_3$*	C	2173	2206
25	$LaPb_3$	C	1433	1263	57	$YbAl_3$	I	1253	1204	89	$TaIr_3$*	C	2727	2688
26	$CePb_3$	C	1443	1283	58	$YbIn_3$	I	903	1106	90	$SmPd_3$*	C	1893	1766
27	$PrPd_3$	C	1448	1696	59	VZn_3	I	896	897	91	$GdSn_3$*	I	1178	1112
28	$GdIn_3$	C	1453	1384	60	USn_3	I	1623	1599	92	$ErAl_3$*	I	1343	1495
29	$PuSn_3$	C	1471	1377	61	$AlNi_3$	I	1668	1665	93	$ScAl_3$*	I	1593	1662
30	$PrIn_3$	C	1486	1394	62	$NbZn_3$	I	1307	1306	94	YTl_3*	I	1153	1106
31	$CeIn_3$	C	1488	1323	63	$DyPb_3$	I	1153	1111					
32	$NdPd_3$	C	1490	1739	64	$ErGa_3$	I	1233	1196					

[a] See footnotes [a]–[d], Table 1. The predicted or correlated melting points of some Eu- or Yb-containing $AuCu_3$-type compounds are usually too high. This is perhaps due to the unusual electronic structure which causes abnormal valency and cohesive energy for Eu and Yb among the series of rare earth metals.

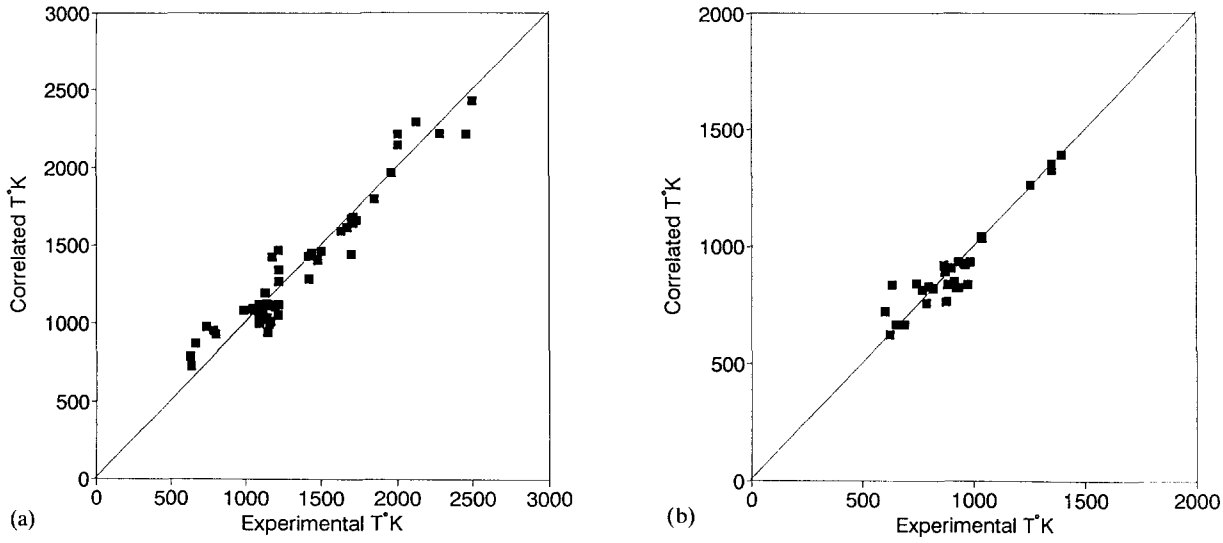

Fig. 8. Correlation between melting point data of AuCuR_3-type alloy phases: (a) congruently melting phase; (b) incongruently melting phase.

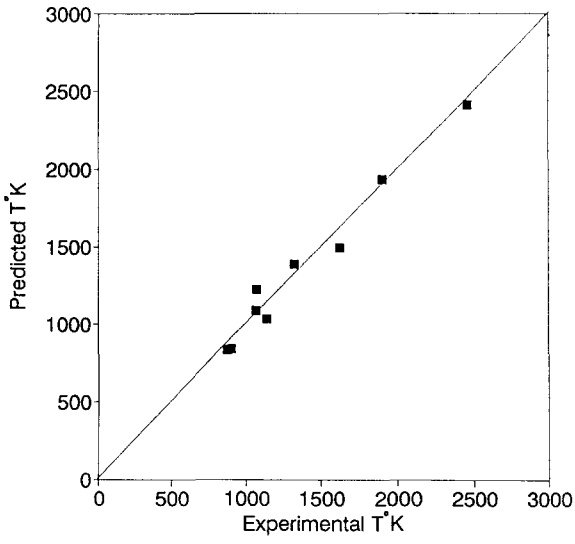

Fig. 9. Computerized predictions of the melting points of nine newly discovered $AuCu_3$-type alloy phases.

$NdSn_3$, $SmPd_3$, $TaIr_3$, $ZrRh_3$, $GdSn_3$, $ErAl_3$, $ScAl_3$ and YTl_3 were predicted by the adjusted ANN (Fig. 9). It can be seen that the predictions were rather good. The average error is <5.4% of the average melting point value.

4. Discussion

We are interested in investigating the influence of each atomic parameter on the melting point of every alloy phase crystal type. This can be done by changing the value of each ANN input while keeping the values of the other inputs unchanged. This kind of computation has been performed for Laves, CsCl-type and $AuCu_3$-type phases. The results are the same: larger ΔX; lower $\Delta(Z/R^3)$; higher melting points for constituent elements tend to make the melting point of alloy phases higher. The influence of geometrical factors is relatively complicated since the radius of an atom may change as charge transfer occurs, but when ΔX approches zero, i.e. when charge transfer is negligible, the optimal R_A/R_B for the closest packing (1.225 for Laves phases, 1.00 for $AuCu_3$-type phases, and 0.73 for CsCl-type alloy phases) indeed tends to correspond to the highest melting points. These empirical relationships agree qualitatively with our model and with the arguement described above.

The semi-empirical method of melting point estimation using an artificial neural network with atomic parameters as inputs has proven to also be useful for many other crystal-types of alloy phases, including prediction of the melting points of the alloy phases with $CaCu_5$-type and $NaZn_{13}$-type crystal structure.

Acknowledgments

This work was supported by the Chinese National High Technology Project and the National Nature Science Foundation of China.

References

[1] F. Hulliger and P. Villars, *J. Alloys Comp., 197* (1993) 197.
[2] U. Walzer, *Phys. Status Solidi B, 162* (1990) 75; *168* (1991) 397.
[3] J.J. Hopfield, *Artificial Neural Networks, IEEE Circuit and Devices Mag., 11* (1988) 3.
[4] A.R. Miedema, *J. Less-Common Met. 32* (1973) 117.
[5] C. Nianyi, L. Chonghe, Y. Shuwen and W. Xueye, *J. Alloys Comp.*, in press.
[6] T.B. Massalski, *Binary Alloy Phase Diagrams*, Am. Soc. Metals, Metal Parks, 1986.